

Single-photon and photon pair emission from MOVPE-grown In(Ga)As quantum dots: shifting the emission wavelength from 1.0 to 1.3 μm

Jan Kettler¹ · Matthias Paul¹ · Fabian Olbrich¹ · Katharina Zeuner¹ · Michael Jetter¹ · Peter Michler¹

Received: 31 July 2015 / Accepted: 14 October 2015 / Published online: 10 March 2016
© Springer-Verlag Berlin Heidelberg 2016

Abstract InAs quantum dots grown on a GaAs substrate have been one of the most successful semiconductor material systems to demonstrate single-photon-based quantum optical phenomena. In this context, we present the feasibility to extend the low-temperature photoluminescence emission range of In(Ga)As/GaAs quantum dots grown by metal-organic vapor-phase epitaxy from the typical window between 880 and 960 nm to wavelengths above 1.3 μm . A low quantum dot density can be obtained throughout this range, enabling the demonstration of single- and cascaded photon emission. We further analyze polarization-resolved micro-photoluminescence from a large number of individual quantum dots with respect to anisotropy and size of the underlying fine-structure splittings in the emission spectra. For samples with elevated emission wavelengths, we observe an increasing tendency of the emitted photons to be polarized along the main crystal axes.

1 Introduction

Benefitting from a wide range of available materials, semiconductor quantum dots (QDs) are generally considered flexible nanostructures with the possibility to tailor their optical properties according to the application requirements [1]. Among

other material systems InAs/GaAs QDs have been most intensely studied and employed for the demonstration of many quantum optical applications in a solid-state environment. Such are, e.g., the emission of single photons [2], two-photon interference [3], the creation of cascaded [4] and entangled photons [5–8] and the entanglement of QD spins with photons [9, 10]. While most of the research has been carried out with QDs emitting from 880 to 960 nm, owing to the GaAs-based growth and the availability of efficient single-photon detectors, the recent years have shown growing attention to the wavelength range above 1 μm . This spectral domain supports the combination of QD single photons with silicon photonic circuits [11] and enables low-loss transmission through optical glass fibers [12]. While InAs/GaAs QDs fabricated by molecular beam epitaxy have been able to reproduce many excellent results at emission wavelengths above 1 μm [13–16], the efforts with QDs grown by metal-organic vapor-phase epitaxy (MOVPE) have been quite limited in numbers [17–19], being restricted in most cases to semiconductor laser-related research. In this study, we demonstrate the feasibility to shift the emission wavelength of MOVPE-grown In(Ga)As QDs from 1.0 to 1.3 μm while maintaining low QD densities. We confirm that the QDs remain excellent single-photon emitters with the possibility to create cascaded photon pairs. We further observe that the fine-structure splittings (FSS) in the QD emission spectra remain reasonably small over the whole wavelength range and the polarization of the fine-structure components tends to predominantly align along the main crystal axes for the samples with elevated emission wavelengths.

This paper is part of the topical collection “Quantum Repeaters: From Components to Strategies” guest edited by Manfred Bayer, Christoph Becher and Peter van Loock.
Jan Kettler and Matthias Paul contributed equally to this article.

✉ Jan Kettler
j.kettler@ihfg.uni-stuttgart.de

¹ Institut für Halbleiteroptik und Funktionelle Grenzflächen, Research Centers SCoPE and IQST, University of Stuttgart, Allmandring 3, 70569 Stuttgart, Germany

2 Sample design

Basically, three knobs can be efficiently used to adjust the confining potential of a QD: size, strain and material

composition. In the context of QD-based semiconductor lasers, many concepts have been introduced to manipulate these properties to lower the emission energy of InAs QDs. Such are, e.g., embedding the QDs in an InGaAs quantum well (dot-in-a-well structures) [20], growth on InP substrates [21] or InGaAs metamorphic buffers [22]. In this study, we employ two concepts: (1) We cover the QDs with a thin In-rich InGaAs layer. (2) We deposit InGaAs as QD material. The InGaAs cover layer results, first, in an effective enlargement of the buried QDs and, second, in the reduction in strain between QDs and the GaAs cap [23] (and is therefore referred to as strain-reducing layer, SRL). Further, the reduced lattice mismatch between QDs and substrate due to the specific alloying of InAs with additional Ga during the QD growth leads for the presented samples to the formation of larger, and less strained QDs with a reduced ground-state energy, obviously dominating over the increased band gap energy, as expected from bulk InGaAs.

The structures are fabricated in a standard horizontal-flow reactor at a pressure of 100 mbar. The QD material of each sample is deposited on a GaAs surface at a temperature of 530 °C. Samples A and B contain InAs QDs without additional Ga. However, an intermixing of In and Ga atoms at the QD-GaAs interface during consecutive growth steps at 610 °C cannot be avoided. The QDs of samples C and D comprise of InGaAs with a nominally equal number of In and Ga atoms. Due to different incorporation rates—depending, among others, on the local strain situation—the In content in the QDs exhibits a gradient, increasing from bottom to top [23]. The amount of deposited monolayers and the V/III ratio are adjusted to obtain low lateral QD densities: For InAs QDs, this is usually obtained by depositing two monolayers, while for InGaAs QDs the amount of deposited material has to be increased by a factor of 3–4. The QDs of samples B, C and D are covered with a 4-nm-thick InGaAs SRL with an In content of 0.13, 0.13 and 0.16, respectively. A scheme of the basic structures used in this work is shown in Fig. 1a. For each sample, an Al(Ga)As/GaAs distributed Bragg reflector (DBR) is applied as bottom mirror, thus enhancing the photon collection efficiency. Sample A comprises an additional top-DBR forming a planar micro-cavity adjusted to the emission wavelength of the QD ensemble.

A profile of an InGaAs QD, as employed in samples C and D, has been obtained by atomic force microscopy (AFM) from an uncapped sample and is shown in Fig. 1b. With a mean diameter of 40 nm and a height of about 9 nm, the InGaAs QDs tend to be higher than their conventional MOVPE-grown InAs counterparts [23, 24], though it should be pointed out that subsequent overgrowth of the QD layer may have dissimilar effects on pure InAs and InGaAs alloyed QDs.

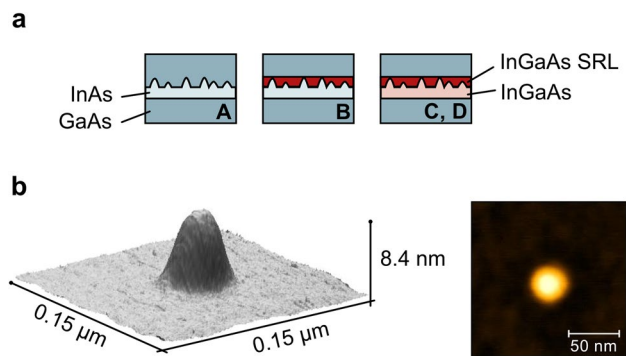


Fig. 1 **a** Sketches of the four sample variations: InAs QDs (A), InAs QDs with SRL (B) and InGaAs QDs with SRL (C, D). Samples C and D differ in the SRL In concentration. **b** AFM height profile of a single InGaAs QD

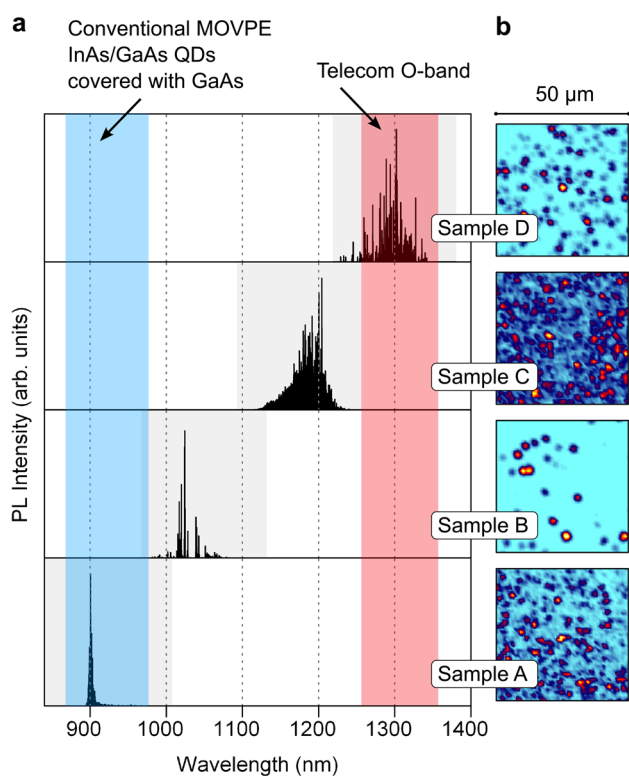


Fig. 2 **a** Quasi-ensemble spectra of samples A to D obtained from a $50\ \mu\text{m} \times 50\ \mu\text{m}$ scanning area. PL is detected over a 160 nm spectral range indicated by the *gray shading*. For sample A, the width of the PL from the QD ensemble is governed by the planar microcavity structure. **b** PL intensity maps of the respective scanning areas. The *color scale* corresponds to the maximum emission intensity within the same spectral range as given in **a**

3 Micro-photoluminescence

For the analysis of the QD micro-photoluminescence (μ -PL), the samples were mounted in a scanning confocal

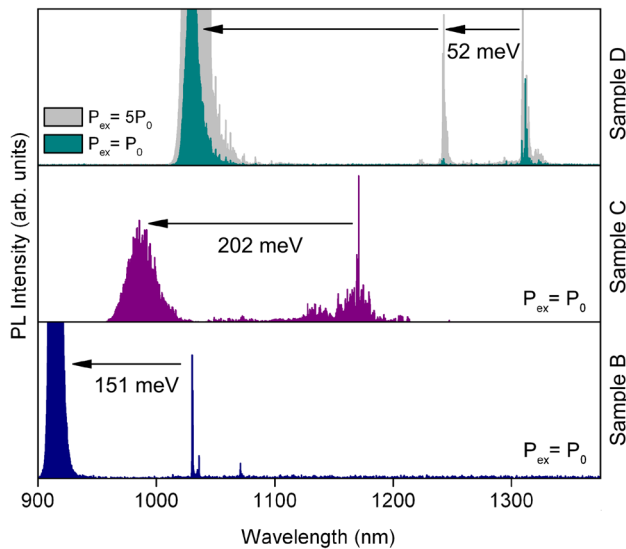


Fig. 3 μ -PL spectra of single QDs and WL of samples B to D. The gray overlay shown for sample D corresponds to a higher excitation power which gives indication for PL emission from the QD p-shell

microscope ($NA = 0.6$) and cooled to 5 K in a liquid-helium flow cryostat. A HeNe laser was used for non-resonant excitation via the GaAs barrier material. The emitted QD photons were analyzed with a 0.5 m monochromator equipped with an InGaAs CCD sensitive to wavelengths from 0.9 to 1.6 μm .

The impact of the different sample designs manifests by means of μ -PL scans of the QD ensembles, as shown in Fig. 2a. For each sample, a “quasi”-ensemble spectrum is obtained by adding up noise-reduced μ -PL spectra from all individual QDs within a $50 \mu\text{m} \times 50 \mu\text{m}$ scanning area. Red-shifted PL is observed, as expected, for sample variations B to D, with the larger and less strained InGaAs QDs emitting more to the long-wavelength side than their “pure” InAs counterparts. The influence of the SRL becomes obvious comparing samples A and B, shifting the conventional InAs QDs from 900 nm (GaAs-covered) to 1030 nm (InGaAs-covered). This effect can be further enhanced by increasing the SRL In content, as demonstrated by changing from sample C to D: here, the red-shift from 1.2 to 1.3 μm corresponds to In contents of 0.13 and 0.16, respectively.

Figure 2b displays μ -PL maps corresponding to each quasi-ensemble spectrum given in Fig. 2a. In combination with AFM measurements [25], we estimate the QD density to be below 10^8 cm^{-2} throughout the wavelength range from 1.0 to 1.3 μm , reaching 10^7 and 10^6 cm^{-2} for samples D and B, respectively.

μ -PL measurements of a single dot on the sample are shown in Fig. 3. For all samples, we observe emission from a quantum well-like feature that we assign mainly to the

QD wetting layer (WL), since the spectral position is essentially affected by the QD material (comparing samples B and C) and only minor by the variation of the SRL In content (comparing samples C and D). Transmission electron microscope measurements of similar samples further suggest that the SRL does not form a coherent quantum well as it is disrupted by the QDs and subjected to thickness fluctuations [23]. Hence, we do not observe any additional contribution to the PL emission of the WL.

The reduction in the QD ground-state energy results in a large spectral gap between QD and WL (approx. 150–250 meV), suggesting strong carrier confinement at low temperatures. For the sample with the strongest confinement, a higher excitation power reveals spectral features, on average 52 meV above the QD ground state. We attribute this to the presence of a p-shell. A closer investigation of the QD ground-state transition shows that the width of the prominent QD lines is less than $95 \mu\text{eV}$ for sample B and less than $77 \mu\text{eV}$ for samples C and D.

4 Single-photon and cascaded photon emission

One of the appealing properties of the samples under investigation lies in the perspective of the application as a telecom-wavelength source of non-classical light. We therefore analyze the second-order autocorrelation function to verify the single-photon nature of the emitted light. The setup we utilize consists of a fiber-based Hanbury-Brown and Twiss (HBT) interferometer with efficient photon detection at wavelengths above 1.0 μm obtained by superconducting single-photon detectors (SSPDs). Figure 4a displays spectra of three single QDs from samples B to D with emission at 1.03, 1.2 and 1.3 μm , respectively. Coincidence histograms of the photon arrival times of each QD exciton (X) transition (Fig. 4b) show a clear antibunching at zero time delay demonstrating pure single-photon emission from all types of red-shifted QDs.

The second-order autocorrelation function $g^{(2)}(\tau) = 1 - (1 - g)e^{-|\tau|/\tau_d}$ has been fitted to the experimental data. Detector dark counts (25 s^{-1}) and timing jitter (70 ps) of the employed SSPDs were sufficiently small to omit any corrections to the correlation data.

The PL intensities we observe from the brightest QD lines of samples B to D are very similar and peak for triggered photon emission at detector count rates of approximately 10 kHz at a 50 MHz excitation rate. Considering the efficiency of the detection setup (1.55 %), the rate of photons collected with the first lens reaches 0.65 MHz corresponding to an extraction efficiency of 1.3 % from a planar sample structure. However, we point out that due to the non-resonant excitation process we simultaneously observe multiple charge configurations of the QD in (time

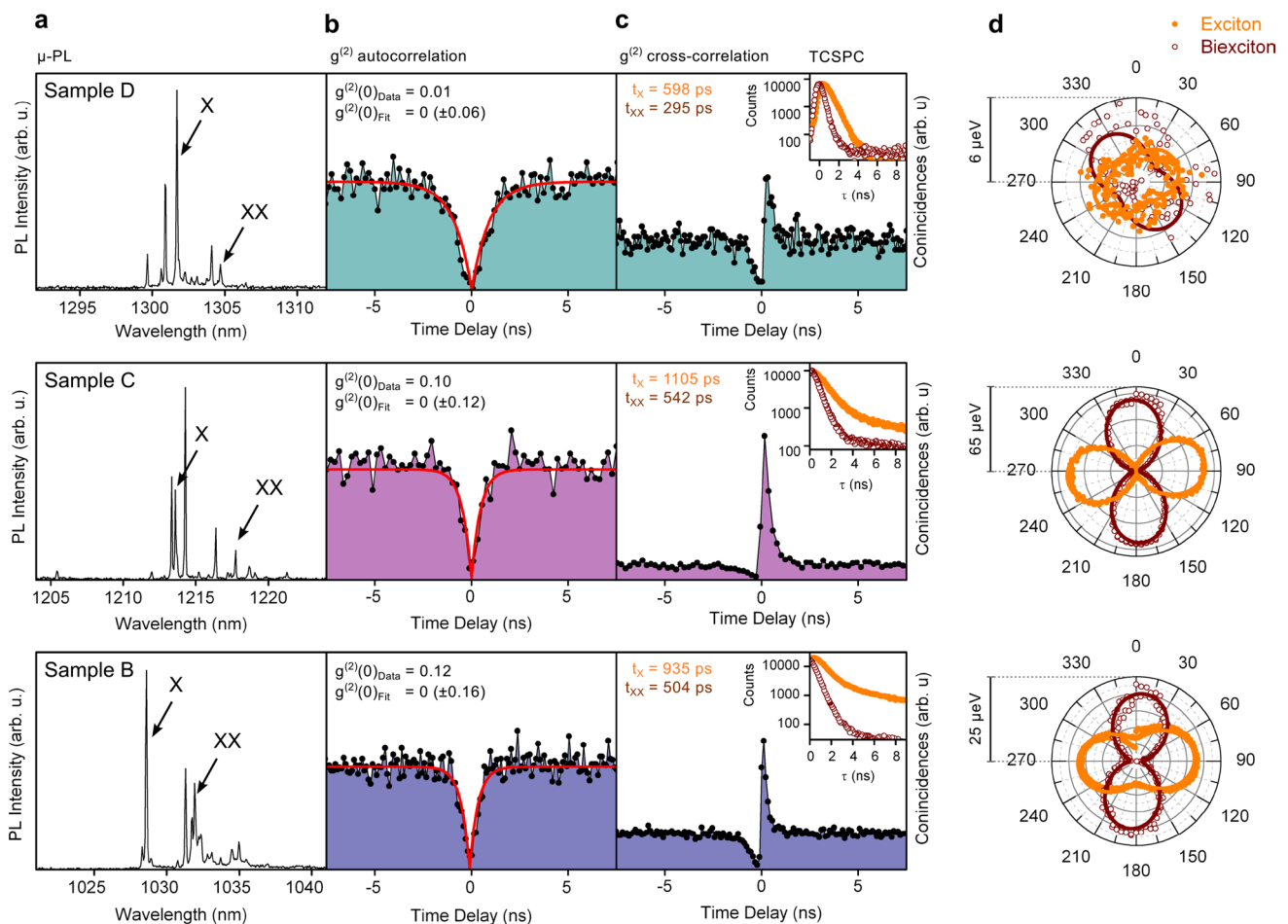


Fig. 4 Demonstration of single-photon and cascaded photon emission for samples B to D. **a** μ -PL spectra with exciton (X) and biexciton (XX) transition lines. **b** Second-order autocorrelation measurements for the exciton line. **c** Intensity cross-correlation measurements

of biexciton (start) and exciton photons (stop). *Inset* Exciton and biexciton decay times obtained by time-correlated single-photon counting (TCSPC). **d** Polarization-dependent energy shifts of exciton and biexciton emission lines

integrated) PL spectra. Thus, the observed count rate from the exciton recombination may be lowered according to the occupation probability of other charge states.

We further show that cascaded photon emission can be observed from samples B to D, which is a prerequisite for the generation of entangled photon pairs from a QD. Evidence is found by feeding photons from different spectral features into the detection channels of the HBT setup. A radiative cascade from two states of a single quantum emitter results in a pronounced elevation of coincidences close to the characteristic anti-bunching dip, as shown by intensity cross-correlation histograms in Fig. 4c. For all of the displayed QDs, the biexciton (XX) photons triggered the start event of the correlation. Pairs of exciton and biexciton have been selected through power- and polarization-resolved μ -PL spectroscopy, filtering pairs of QD lines with similar FSS and converse polarization axes of high- and low-energetic components. The exciton and biexciton

energy splittings are obtained through selecting a distinct fine-structure component by polarization and carefully fitting the μ -PL emission line [26], as shown in Fig. 4d. The precision of this method is strongly dependent on the background of an individual μ -PL spectrum and otherwise limited by the signal-to-noise ratio (SNR) of the complete series. For the assigned exciton–biexciton pairs given in Fig. 4 we find biexciton binding energies of 3.9, 3.5 and 2.2 meV (sample B to D) which match the energy range of comparable MBE grown QDs [27, 28].

We determined exciton and biexciton lifetimes by means of time-correlated single-photon counting statistics (TCSPC) using a pulsed laser ($f_{ex} = 50$ MHz) for non-resonant excitation at 650 nm. The decay rates for the exciton approximately double the rates of the biexciton (see insets Fig. 4). On average, sample D exhibits comparatively fast exciton life times (~ 550 ps), while samples B and C (~ 960 , ~ 1050 ps) agree very well with In(Ga)As QDs

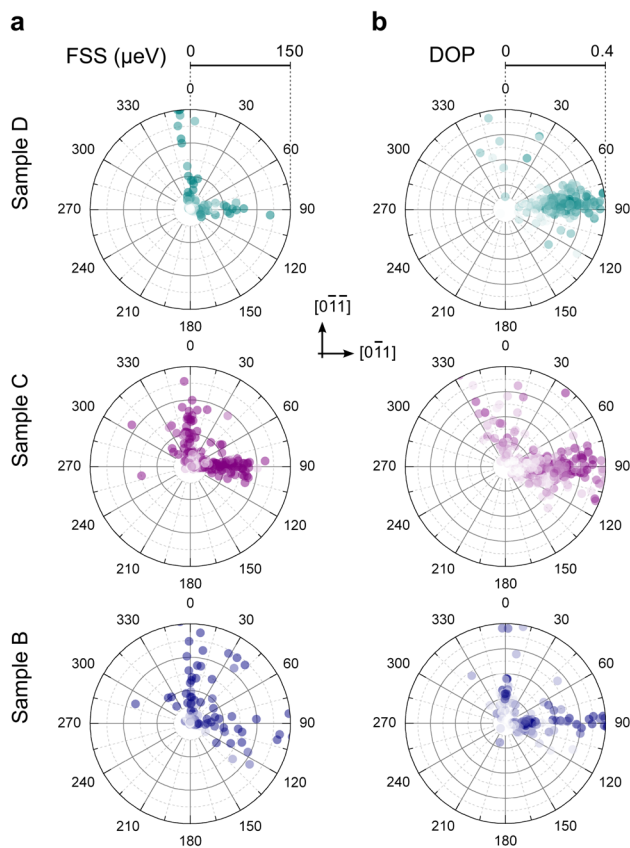


Fig. 5 Polarization-resolved μ -PL studies. Every data point refers to a single spectral line. The *color* density relates to the SNR of the corresponding data set. **a** FSS as a function of the polarization orientation of the high-energy component of the split doublet. **b** Degree of linear polarization (DOP) over the polarization angle

emitting below 1 μm . Whether the origin of the reduced lifetimes relates to an enhanced oscillator strength or to the presence of non-radiative decay channels requires further extensive investigation.

5 Polarization anisotropy

As the generation of polarization-entangled photon pairs via the biexciton–exciton cascade greatly benefits from QDs with low or zero FSS, we analyzed the polarization-resolved μ -PL from a large number of QDs in the same way as described with respect to Fig. 4d. For the analysis, all spectral lines observable from each non-resonantly excited QD spectrum have been considered, thus involving also trions with zero splittings and states with larger FSS as, e.g., excited trions or charged biexcitons. Figure 5a shows all extracted splittings as a function of the polarization axis of the high-energetic component. We find that the QDs show an increasing tendency to align along the $[0\bar{1}1]$ and $[0\bar{1}\bar{1}]$ crystal axes from sample B to D. A similar trend

is observed for the anisotropy of the PL intensity, exhibiting a clear maximum along the $[0\bar{1}1]$ axis, as shown in Fig. 5b. Although this suggests an increased elliptical shape of long-wavelength QDs, we cannot verify this by AFM measurements.

Despite large variations of FSS from zero to 200 μeV , we find a more or less homogenous distribution of splittings down to a few μeV , indicating the QDs are suitable for post-growth FSS tuning techniques as demonstrated, e.g., in Ref. [29], by combining mechanical strain and an electrical field. Moreover, the pronounced alignment along the crystal axes, as observed for sample D, should be beneficial for even simpler techniques [30] based on uniaxial strain only.

6 Conclusion

In summary, we have demonstrated that MOVPE-grown In(Ga)As/GaAs QDs can be tailored to emission wavelengths ranging from 1.0 to 1.3 μm without strongly varying properties from conventional In(Ga)As QDs. A low QD density allowed the verification of single-photon and cascaded photon emission from the biexciton–exciton cascade for all red-shifted QD samples. With the addition of further post-growth FSS tuning techniques, we consider these QDs to be promising candidates for future telecom sources of entangled photon pairs.

Acknowledgments The authors gratefully acknowledge funding by the Federal Ministry of Education and Research, in particular for the projects Q.com-H (16KIS0115) and QuaHL-Rep (01BQ1041).

References

1. P. Michler (ed.), *Single Quantum Dots, Topics in Applied Physics*, vol. 90, 1st edn. (Springer, Berlin Heidelberg, 2003)
2. P. Michler, A. Kiraz, C. Becher, W.V. Schoenfeld, P.M. Petroff, L. Zhang, E. Hu, A. Imamoglu, *Science* **290**(5500), 2282 (2000)
3. C. Santori, D. Fattal, J. Vucković, G.S. Solomon, Y. Yamamoto, *Nature* **419**, 594 (2002)
4. E. Moreau, I. Robert, L. Manin, V. Thierry-Mieg, J. Gérard, I. Abram, *Phys. Rev. Lett.* **87**, 183601 (2001)
5. N. Akopian, N.H. Lindner, E. Poem, Y. Berlatzky, J. Avron, D. Gershoni, B.D. Gerardot, P.M. Petroff, *Phys. Rev. Lett.* **96**, 130501 (2006)
6. R.J. Young, R.M. Stevenson, P. Atkinson, K. Cooper, D.A. Ritchie, A.J. Shields, *N. J. Phys.* **8**(29), 2 (2006)
7. R. Hafenbrak, S.M. Ulrich, P. Michler, L. Wang, A. Rastelli, O.G. Schmidt, *N. J. Phys.* **9**(9), 315 (2007)
8. H. Jayakumar, A. Predojević, T. Kauten, T. Huber, G.S. Solomon, G. Weihs, *Nat. Commun.* **5**, 4251 (2014)
9. K. De Greve, L. Yu, P.L. McMahon, J.S. Pelc, C.M. Natarajan, N.Y. Kim, E. Abe, S. Maier, C. Schneider, M. Kamp, S. Hofling, R.H. Hadfield, A. Forchel, M.M. Fejer, Y. Yamamoto, *Nature* **491**(7424), 421 (2012)
10. W.B. Gao, P. Fallahi, E. Togan, J. Miguel-Sanchez, A. Imamoglu, *Nature* **491**(7424), 426 (2012)

11. E. Murray, D.P. Ellis, T. Meany, F.F. Flother, J.P. Lee, J.P. Griffiths, G.A.C. Jones, I. Farrer, D.A. Ritchie, A.J. Bennet, A.J. Shields, *Appl. Phys. Lett.* **107**(17), 171108 (2015). <http://dx.doi.org/10.1063/1.4935029>
12. E.F. Schubert, T. Gessmann, J.K. Kim, *Light Emitting Diodes* (Wiley, New York, 2005)
13. M.B. Ward, O.Z. Karimov, D.C. Unitt, Z.L. Yuan, P. See, D.G. Gevaux, A.J. Shields, P. Atkinson, D.A. Ritchie, *Appl. Phys. Lett.* **86**(20), 201111 (2005)
14. B. Alloing, C. Zinoni, V. Zwiller, L.H. Li, C. Monat, M. Gobet, G. Buchs, A. Fiore, E. Pelucchi, E. Kapon, *Appl. Phys. Lett.* **86**(10), 101908 (2005)
15. M.T. Rakher, L. Ma, O. Slattery, X. Tang, K. Srinivasan, *Nat. Photon.* **4**(11), 786 (2010)
16. M.B. Ward, M.C. Dean, R.M. Stevenson, A.J. Bennett, D.J.P. Ellis, K. Cooper, I. Farrer, C.A. Nicoll, D.A. Ritchie, A.J. Shields, *Nat. Commun.* **5**, 3316 (2014)
17. N.I. Cade, H. Gotoh, H. Kamada, H. Nakano, H. Okamoto, *Phys. Rev. B* **73**, 115322 (2006)
18. T. Yamaguchi, T. Tawara, H. Kamada, H. Gotoh, H. Okamoto, H. Nakano, O. Mikami, *Appl. Phys. Lett.* **92**(8), 81906 (2008)
19. D. Guimard, H. Lee, M. Nishioka, Y. Arakawa, *Appl. Phys. Lett.* **92**(2008), 163101 (2008)
20. V.M. Ustinov, N.A. Maleev, A.E. Zhukov, A.R. Kovsh, A.Y. Egorov, A.V. Lunev, B.V. Volovik, I.L. Krestnikov, Y.G. Musikhin, Na Bert, P.S. Kopev, Z.I. Alferov, N.N. Ledentsov, D. Bimberg, *Appl. Phys. Lett.* **74**(19), 2815 (1999)
21. B. Lambert, A. Corre, V. Drouot, H. L'Haridon, S. Loualiche, *Semicond. Sci. Technol.* **13**(1), 143 (1998)
22. A. Bosacchi, P. Frigeri, S. Franchi, P. Allegri, V. Avanzini, J. Cryst. Growth **175–176 Part 2**, 771 (1997)
23. E. Goldmann, M. Paul, F.F. Krause, K. Müller, J. Kettler, T. Mehrrens, A. Rosenauer, M. Jetter, P. Michler, F. Jahnke, *Appl. Phys. Lett.* **105**, 152102 (2014)
24. D. Richter, R. Hafenbrak, K.D. Jöns, W.M. Schulz, M. Eichfelder, M. Heldmaier, R. Roßbach, M. Jetter, P. Michler, *Nanotechnology* **21**(12), 125606 (2010)
25. M. Paul, J. Kettler, K. Zeuner, C. Clausen, M. Jetter, P. Michler, *Appl. Phys. Lett.* **106**(12), 122105 (2015)
26. K. Kowalik, O. Krebs, A. Lematre, S. Laurent, P. Senellart, P. Voisin, J.A. Gaj, *Appl. Phys. Lett.* **86**(4), 041907 (2005)
27. A. Schliwa, M. Winkelkemper, D. Bimberg, *Phys. Rev. B* **79**, 075443 (2009)
28. M. Wimmer, S.V. Nair, J. Shumway, *Phys. Rev. B* **73**, 165305 (2005)
29. R. Trotta, E. Zallo, C. Ortix, P. Atkinson, J.D. Plumhof, J. van den Brink, A. Rastelli, O.G. Schmidt, *Phys. Rev. Lett.* **109**, 147401 (2012)
30. J. Zhang, J.S. Wildmann, F. Ding, R. Trotta, Y. Huo, E. Zallo, D. Huber, A. Rastelli, O.G. Schmidt, *Nat. Commun.* **6**, 10067 (2015). <http://dx.doi.org/10.1038/ncomms10067>